

Polyethylene-based single polymer laminates: Synergistic effects of nanosilica and metal hydroxides

Journal of Reinforced Plastics and Composites
2019, Vol. 38(2) 62–73
© The Author(s) 2018
Article reuse guidelines:
sagepub.com/journals-permissions
DOI: 10.1177/0731684418802974
journals.sagepub.com/home/jrp


Andrea Dorigato¹, Giulia Fredi¹ , Luca Fambri¹,
José-Marie Lopez-Cuesta² and Alessandro Pegoretti¹

Abstract

This work aims to investigate the fire performance of novel polyethylene-based single polymer composites. Fumed silica nanoparticles and magnesium hydroxide microfiller were added at an optimized concentration to a linear low-density polyethylene matrix, which was then reinforced with ultra-high molecular weight polyethylene fibers. Through the optimization of the production process, it was possible to limit the porosity inside the single polymer composites, thus retaining the pristine mechanical properties of the fibers. The addition of SiO₂ and magnesium hydroxide determined an increase in the elastic modulus in both the longitudinal and transversal direction, but it concurrently led to a reduction in ductility, especially in the transversal direction. The fillers were proved to bring interesting improvements of the thermal degradation resistance and of the flame behaviour. Thermogravimetric analysis tests highlighted an increase in the onset degradation temperature and in the temperature associated to the maximum degradation rate. Moreover, both the oxidation onset temperature and limiting oxygen index were considerably improved. Cone calorimetry tests evidenced that filled single polymer composites were characterized by lower peak heat release rate and total heat released with respect to neat single polymer composites.

Keywords

Fumed silica, polyethylene, nanocomposites, fire retardants, single polymer composites

Introduction

Thanks to their peculiar combination of low density, high processability and interesting physical properties, polymers and polymer-matrix composites have found a massive application in several fields, such as automotive and aerospace components.^{1,2} In particular, polyethylene (PE) is one of the most widely used thermoplastics because of its combination of high chemical resistance, good mechanical properties and cheapness. Among the PE types, linear low-density polyethylene (LLDPE) is widely used in film and packaging industry for its high impact and tear strength and easy drawability.^{1,3,4} As a drawback, polymers are generally characterized by elevated flammability, with the consequent production of toxic gases and smoke during combustion. Therefore, the improvement of their flame resistance is a key point to further extend their applicability and to meet the current safety requirements.^{2,5,6}

In order to improve the fire resistance of polyolefins, the most widely adopted approach is to add flame

retardants (FRs). These fillers, acting physically and/or chemically in the solid, liquid or gas phase, are able to hinder combustion through different mechanisms which act on different aspects of fire generation and propagation (heat source, ignition, thermal decomposition, smoke production and composition, flame spread).⁷ The most common FRs are represented by metal hydroxides, boron-based FRs, halogen-based FRs, phosphorous-based FRs, silicon-based FRs, nitrogen-based FRs, intumescent fillers and nanometric

¹Department of Industrial Engineering and INSTM Research Unit, University of Trento, Trento, Italy

²Ecole des Mines d'Alés (C2MA), Alès Cedex, France

Corresponding author:

Andrea Dorigato, Department of Industrial Engineering and INSTM Research Unit, University of Trento, Via Sommarive 9, 38123 Trento, Italy.

Email: andrea.dorigato@unitn.it

particles.⁶ Even though halogenated FRs based on Cl or Br are able to impart good fire performance even at very low concentrations, their application has been restricted in various regions because of their tendency to form toxic components (i.e. dioxins and furans) and to form corrosive gases that can damage metal parts and electronic components.^{8–10} Therefore, one of the most diffused classes of halogen-free FRs is represented by the metal hydroxides, such as aluminum trihydroxide ($\text{Al}(\text{OH})_3$) and magnesium hydroxide ($\text{Mg}(\text{OH})_2$).^{11,12} These fillers are available on the market mainly as micrometric particles to be additivated to polymer matrices at elevated concentrations. Through an endothermic decomposition, in a certain temperature interval (possibly close to the polymer decomposition temperature), they are able to produce a temperature decrease, thereby slowing the thermal degradation process.¹³ The produced metal oxides and water dilute the combustible gas mixture, limiting the reagents concentration in the gas phase and the ignition probability. The protective barrier layer created by this metal oxide physically separates the oxygen from the combustible gases and limits the smoke generation.^{7,13–15} As a drawback, a high FRs loading (in certain cases more than 40 wt%) is required to appreciably increase the flame resistance of the resulting materials, with negative effects on the processability and the ductility of the polymer.^{12,13,16–20} In order to overcome this heavy limitation, it is possible to partially replace metal hydroxides with another filler with FR properties (i.e. nanoclay,^{21,22} zinc borate²³ and fullerene (C_{60})²⁰). If the selected fillers act synergistically, the same flame resistance can be achieved with a lower FR amount.⁶ Among the nanofillers used as FRs, fumed silica has been investigated either alone or in combination with other FRs.^{24–28} Due to its fractal structure and its high specific surface area, fumed silica is prone to self-aggregation and can consequently form a network of connected or interacting particles in polymer matrices.²⁹ In a recent paper of our group,³⁰ various amounts of surface-treated fumed silica nanoparticles were melt compounded with a high-density PE matrix, in order to study the thermal resistance and flammability properties of the resulting nanocomposites. The results of thermogravimetric analysis (TGA) highlighted the capability of the selected nanoparticles in increasing the decomposition temperature and in decreasing the mass loss rate, while limiting oxygen values were noticeably improved with respect to the unfilled matrix. Moreover, functionalized nanoparticles revealed extremely effective in delaying the time to ignition and in suppressing the heat release rate (HRR) values, while the presence of an evident matrix charring for nanofilled sample only slightly increased the quantity of smoke produced.

Even though the synergistic effect of nanoparticles and other FRs has been investigated in many research works, only few papers are available in the open scientific literature on the flame-retardancy enhancement due to the combination of metal hydroxides and iso-dimensional fillers, such as fumed silica nanoparticles.^{3,30–32} In a recent paper of our group,³³ LLDPE-based micro/nano-composites were prepared by using surface-functionalized fumed silica nanoparticles and two kinds of metal hydroxides (aluminum trihydroxide and $\text{Mg}(\text{OH})_2$) at different relative amounts, with the aim to investigate the FR capability to improve the fire resistance, the thermal degradation performance and the mechanical properties of the matrix, and to evaluate possible synergistic effects between the selected micro- and nanofillers. Limiting oxygen index (LOI) and cone calorimetry tests on the samples with optimized compositions demonstrated that the synergistic effect between $\text{Mg}(\text{OH})_2$ and fumed silica at a proper relative ratio could lead to a strong enhancement of both the LOI values and of the cone calorimetry performance. The scientific outcomes of this work constitute the basis for the subject of the present work in which a LLDPE nanocomposite with optimized composition was used as matrix for fire-resistant PE-based single polymer composites (SPCs).

SPCs, also known as one-polymer composites, homocomposites, all polymer composites, self-reinforced or homogeneous composites, are characterized by the fact that both the matrix and the reinforcement have the same chemical composition.³⁴ If there is a significant difference between the melting temperature of the matrix and of the fibers (i.e. a processing window), it is possible to produce SPCs that can be entirely re-melted (and thus thermally recycled) at the end of their service life.³⁵ Moreover, the interfacial bonding can be considerably improved when the matrix and the reinforcement have the same chemical nature.^{36,37} Starting from the first example of all-PE composites developed by Capiati and Porter,³⁸ in 1975, many efforts were devoted to explore new materials combinations and processing techniques. The literature reports many examples of PE,³⁹ polypropylene,⁴⁰ poly(ethylene terephthalate),⁴¹ poly(methyl methacrylate),⁴² poly(ethylene naphthalate)⁴³ and liquid crystalline copolyesters⁴⁴ SPCs. However, only few works can be found on the study and the improvement of the thermal degradation resistance and fire performance of SPCs. Bocz et al.^{45,46} developed and characterized a flame-resistant all-polypropylene composite with self-extinguishing properties, where the FR was ammonium polyphosphate. Seyhoglu and Dogan⁴⁷ introduced two kinds of organophosphorous-based FR additive to improve the fire performance of a polyamide-based SPC.

The aim of this work is to develop novel PE-based SPCs with improved FR properties. To the best of our knowledge, this is the first example of flame-resistant SPC based on PE. Two different polymer matrices (i.e. neat LLDPE and a nanofilled LLDPE with optimized composition) were reinforced with ultra-high molecular weight PE (UHMWPE) fibers. The nanocomposite formulation based on $Mg(OH)_2$ and fumed silica was properly selected for its interesting combination of mechanical properties, ductility, processability, thermal resistance and fire performance.³³ After a detailed characterization of the constituents, the most important thermo-mechanical and flame-resistance properties of the prepared SPCs will be investigated.

Materials and methods

Materials

Polymer granules of LLDPE Flexirene[®] CL10 (density = 0.918 g/cm³, melting temperature = 121°C) were provided by Versalis SpA (Milan, Italy). Micrometric particles of $Mg(OH)_2$ Hydrofy[®] G1.5 were purchased by Nuova Sima Srl (Ancona, Italy). This filler has a nominal decomposition temperature of 350°C, a specific gravity of 2.36 g/cm³ and a BET surface area of 9 m²/g. Fumed silica nanoparticles Aerosil[®] r974, surface treated with dimethyldichlorosilane, were supplied by Evonik GmbH (Essen, Germany). Aerosil[®] r974 has a surface area of 170 m²/g, a bulk density of 1.99 g/cm³ and a tap density of 60 g/l. This nanofiller is constituted by equiaxed primary nanoparticles with an average size of 12 nm (SiO_2 content 99.8%), organized in an aggregated structure. The UHMWPE fibers used to produce the SPCs were provided by the company DSM (TE Heerlen, the Netherlands) under the trade name of Dyneema[®] SK99 (density 0.980 g/cm³, filament diameter 12–21 μm). They are high-performance fibers with high strength, low elongation at break, low density and a good chemical resistance. All materials were used as received, without further purification.

Sample preparation

Two types of matrices were considered. The first matrix was made only of neat LLDPE, and the second was composed of LLDPE, $Mg(OH)_2$ (20 wt%) and fumed nanosilica (4.8 wt%). This composition was chosen because it was selected as the optimal formulation on the basis of the results of our previous work on the synergistic effects of metal hydroxides and fumed nanosilica fire retardants for PE.³³ For the preparation of the matrices, polymer granules (and the fillers in one case) were melt compounded in a Thermo Haake

Polylab Rheomix internal mixer at 190°C for 10 min at 90 r/min. To avoid agglomeration, the fillers were slowly added after the complete melting of LLDPE. The resulting composites were then hot-pressed in a Carver laboratory press at 170°C for 10 min, under a pressure of 2.5 MPa, to obtain square sheets of 200 × 200 × 1.5 mm³.

SPCs were prepared with the use of a mandrel around which the Dyneema[®] SK99 fibers (hereafter they will be named DSK99) were unidirectionally wrapped for 80 and 50 times, depending on the dimensions of the specimens required by the tests (i.e. 50 times for cone calorimeter test, which required smaller specimens, and 80 times for all the other analyses). SPCs were made by alternating sheets of matrix with layers of fibers. Each SPC specimen was made by three sheets of polymer matrix and two layers of fibers. SPC specimens wrapped 50 times had dimensions of 170 × 100 × 1.5 mm³, while SPC specimens wrapped 80 times had dimensions of 100 × 100 × 3.5 mm³. The hot compaction process was performed with the same hot-plate press used to produce the matrices. Non-consolidated SPCs were inserted in the press at room temperature. The initial pressure of 1.5 MPa was maintained constant until the machine reached the temperature of 140°C. Once at 140°C, the pressure was increased at 3 MPa for 30 s (total heating time 15 min). Previous works demonstrated that the application of a higher pressure for a limited time does not damage the fibers and promotes a good consolidation of the SPC.⁴⁴ Then, the system was switched off and cooled down at room temperature, under a pressure of 1.5 MPa (total cooling time 15 min). In order to select the pressing temperature (i.e. 140°C), preliminary mechanical tests on single fibers treated at different temperatures (i.e. 135°C and 140°C) for the same time interval utilized in the hot compaction process were performed. In the following sections, the two matrices, the neat LLDPE and that with the FRs with the optimized formulation, will be named as PE and PE composite with optimized composition (OPT), respectively. Neat UHMWPE fibers will be named DSK99, while the SPCs will be denoted as SPC-PE and SPC-OPT, depending on whether the matrix was made by PE or OPT.

Experimental techniques

Characterization of the constituents. X-ray diffraction (XRD) analysis was performed on the PE matrix and on the DSK99 fibers, in order to investigate their crystalline behaviour. The measurements were performed by using two different instruments, i.e. a texture diffractometer prototype based on a Huber goniometer and an Ital structures IPD3000 powder diffractometer.

The first machine, used to characterize the DSK99 fibers, was equipped with a microfocus 50 W Cu source coupled with a two-dimensional elliptic mirror monochromator, a Dectris Eiger 1M 2D hybrid pixel detector and a four-circle goniometer to allow sample rotation around π and χ circles. The sample was loaded in transmission geometry with the fiber parallel to the 2θ goniometer axis. Diffraction images were collected over the 10° – 70° 2θ equivalent range and (0° , 15° , 30° , 45°) π axis orientations, assuming axial symmetry of crystallites orientation. The IPD3000 diffractometer was used to acquire XRD spectra on a neat LLDPE sheet. It was equipped with a 1200 W Co source, a multilayer monochromator and 100 μm slits on the incident beam. The sample was positioned in reflection geometry with a fixed omega angle with respect to the incident beam (5°). Diffraction data were collected by means of an Inel CPS120 detector over 5° – 120° 2θ range (0.03° per channel).

Differential scanning calorimetry (DSC) tests were performed on the PE matrix and on the DSK99 fibers (as received and thermally treated at 135°C and 140°C), in order to evaluate the effect of the processing temperature on the crystalline behaviour of the reinforcing phase. DSC measurements were performed with a Mettler DSC 30 machine. Specimens of approximately 10 mg were tested in the temperature range 0 – 200°C , with a heating/cooling rate of $10^\circ\text{C}/\text{min}$, under a N_2 flux of 100 ml/min. A heating scan, a cooling scan and a second heating scan were performed. In this way, the melting temperature (T_m) and the melting enthalpy (ΔH_m) of the samples were determined. The crystallinity degree (X_c) was calculated with the expression reported in equation (1) as

$$X_c = \frac{\Delta H_m}{\Delta H_0} \cdot 100 \quad (1)$$

where ΔH_0 is the theoretical heat of fusion of the 100% crystalline PE (i.e. 293 J/g).⁴⁸

The mechanical properties of the constituents were investigated through quasi-static uniaxial tensile tests. For the characterization of the matrices, dumbbell 1BA specimens (standard UNI EN ISO 527–2) were die-cut from the prepared sheets and tested with an Instron 5969 universal testing machine, equipped with a 50 kN load cell. For the measurement of the elastic modulus, five specimens were tested for each composition at 0.25 mm/min, with a resistance extensometer Instron 2620–601, having a gauge length of 12.5 mm. The tests were stopped at a strain of 1%, and the elastic modulus was evaluated with the secant method between the strain levels 0.05 and 0.25%. Tensile properties at break were performed at a crosshead speed

of 100 mm/min on 1BA specimens. The resulting stress–strain curves were employed to obtain the values of the elastic modulus (E), of the stress at yield (σ_y), of the stress at break (σ_b) and of the strain at break (ε_b). Tensile tests on single fibers were performed following the ASTM C 1557 standard by using an Instron 4502 machine, equipped with a load cell of 10 N, at a crosshead speed of 1 mm/min. Strain values were recorded without any extensometer. The fibers were glued on paper frames with a gauge length of 20 mm. At least five specimens were tested for each sample.

Characterization of the SPCs. The experimental density of the SPCs laminates was measured with the technique of the Archimedes balance in ethanol⁴⁹ through a Gibertini E42 analytical balance. Thus, a theoretical (ρ_{th}) and an experimental density (ρ_{exp}) could be obtained, and the volume fractions of fibers (φ_f), matrix (φ_m) and voids (φ_v) were subsequently calculated. The density of the constituents (matrix and fibers) was previously determined with a Micromeritics AccuPyc 1330 helium pycnometer at 23°C .

TGA was performed with a TA Instrument Q5000IR, at a heating rate of $10^\circ\text{C}/\text{min}$ from room temperature to 700°C . Specimens of approximately 10 mg were die-cut from the prepared samples tested under an air flux of 15 ml/min. TGA tests were performed in air because the degradation in an oxidizing environment is closer to the real-life conditions in which a flame-retardant agent may operate. From these tests, it was possible to evaluate the temperatures corresponding to onset of the degradation (T_{onset}), determined with the tangent method on the first change in slope of the curve mass-versus-temperature, while the temperature of the maximum degradation rate (T_{peak}) was identified as the maximum of the mass loss derivative as a function of temperature.

Mettler DSC 30 instrument was employed to carry out oxidation onset temperature (OOT) tests. These tests aim to measure the temperature at which the material starts to degrade, under a constant heating rate. Specimens of approximately 10 mg were tested following the ASTM E 2009 standard, under an air flux of 100 ml/min and a heating rate of $10^\circ\text{C}/\text{min}$ from room temperature to 300°C , and the OOT was determined by the tangent method between the baseline and the degradation peak.

Quasi-static tensile tests on SPCs were performed by using an Instron 5969 tensile testing machine. Rectangular specimens of $90 \times 10 \times 1.5 \text{ mm}^3$ were tested at a crosshead speed of 5 mm/min. According to the ISO 527 standard, the Young modulus (E) was evaluated with the secant method between the point 1 and 1.5% of the strain, and also the stress at break (σ_b)

and the strain at break (ϵ_b) were determined. The tensile energy to break value (TEB) was determined as integral under the stress–strain curve. Due to the unidirectionality of the fibers, the tensile properties were determined both in longitudinal (L) and in transversal (T) direction.

LOI tests were performed to measure the minimum oxygen concentration that sustains the combustion process. According to ASTM D 2683 standard, rectangular specimens of $100 \times 10 \times 3 \text{ mm}^3$ were placed vertically inside a CEAST Oxygen Index apparatus. A blowtorch igniter was used to start the combustion process from the top of the specimen. The material is considered able to burn with a given oxygen concentration if the flame is able to top–down burn the specimen for a length of at least 50 mm in 3 min. The flame propagation rate in air (O_2 concentration around 20.8%) was also evaluated by measuring the time needed to burn 50 mm of the specimen.

Cone calorimetry is generally considered as the analysis that provides an all-round characterization of the flame behavior of a material. The technique is based on the measurement of the decreasing oxygen concentration in the combustion gases of a sample subjected to a constant heat flux, which is then used to calculate the heat released per unit time and surface area, the HRR, measured in kW/m^2 .⁶ Cone calorimetry tests were performed with a Fire Testing Technology cone calorimeter following the ISO 5660–1 standard. Square specimens of $100 \times 100 \times 3 \text{ mm}^3$ were tested under a heat flux of 35 kW/m^2 . Besides the HRR value, it was also possible to determine the time-to-ignition,

the total heat released (THR), the peak of the HRR (pHRR) and the mass of the specimens after the tests. The test also allowed the calculation of other parameters, such as the fire performance index (FPI) as the ratio between TTI and pHRR, the fire growth rate (FIGRA) as the maximum in $\text{HRR}(\text{time})/\text{time}$ and the maximum of average heat release emission (mAHRE) as a function of time.

Results and discussion

Characterization of the constituents

In order to understand the properties of the prepared SPCs, it is important to characterize the constituents (i.e. the LLDPE matrix and the fibers). Rietveld modeling was performed on collected diffraction data of both samples by means of the Maud software⁵⁰ taking into account crystalline and amorphous fraction quantification, average crystallite size of the crystalline fraction as well as orientation distribution quantification for the fiber sample. In Figure 1(a) and (b), the results of XRD analysis on the UHMWPE fibers are reported. In particular, in Figure 1(a), a 2D contour map representation of the diffraction spectra collected on the fibers as received is reported, while in Figure 1(b), the (200) pole figure is shown, representing the probability distribution of (h00) planes with respect to the sample coordinate frame. The latter clearly shows a strong preferred orientation of the main cell axis along the fiber direction.

From the quantitative Rietveld analysis, it is possible to obtain the crystallinity degree (X_c) and average

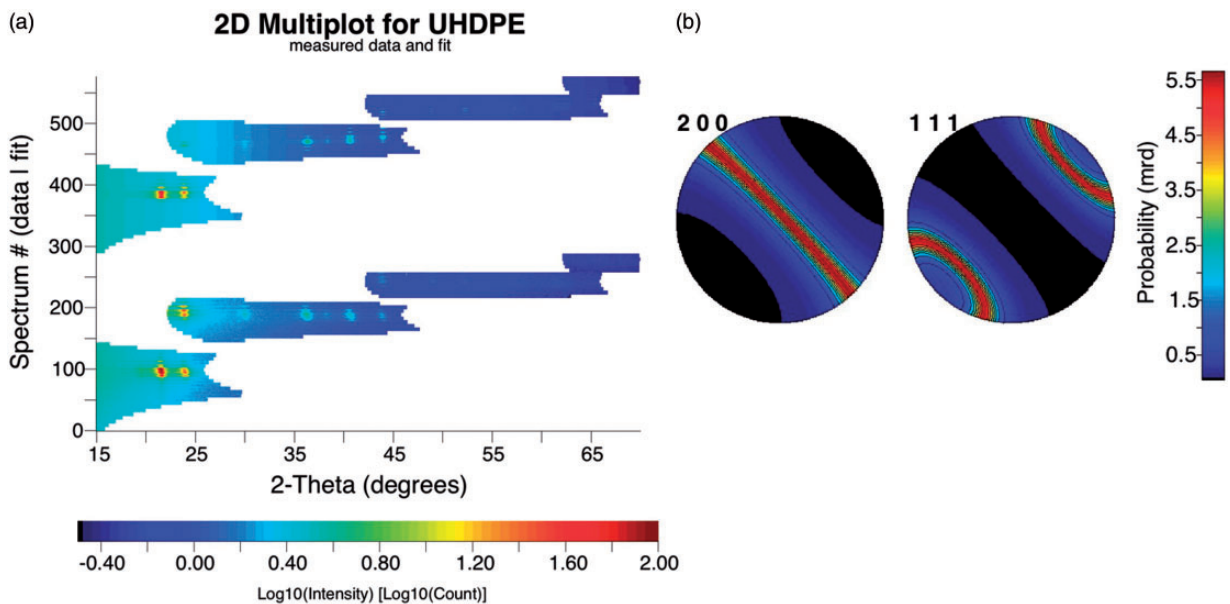


Figure 1. XRD results on UHMWPE fiber: (a) contour map representation of the diffraction spectra (x axis: 2θ , y -axis: ϕ ; bottom: experimental intensities; top: reconstructed intensities) and (b) (200) pole figure.

Table 1. Results of the XRD analysis (crystallinity degree (X_c) and average crystallite size) on neat PE matrix and UHMWPE fibers.

Sample	X_c (%)	Average crystallite size (Å)
PE	48.85	265
DSK99	97.85	350

PE: polyethylene; UHMWPE: ultra-high molecular weight polyethylene; XRD: X-ray diffraction.

crystallite size both of neat PE matrix and of the fibers. As reported in Table 1, the UHMWPE fibers are characterized by elevated crystallinity degree (almost 98%), with crystallites having higher size (about 350 Å). This is not surprising, since during the production process, the fibers are strongly aligned. Together with the higher molecular weight with respect to LLDPE, these features explain the elevated mechanical properties of these fibers.⁵¹

In order to select the most suitable SPCs processing parameters and to determine the influence of the hot-pressing temperature on the physical properties of the reinforcing fibers, it is also important to perform DSC tests. In Table 2, the results of the DSC test on the neat PE matrix and on UHMWPE fibers as received and treated at two different temperatures (135°C and at 140°C) are summarized. As expected, both the melting temperature and the melting enthalpy of the DSK fibers are considerably higher with respect to those of the PE sample. The discrepancy in the crystallinity values with respect to the results reported for XRD tests (see Table 1) is probably due to the difference in the experimental configuration of the tests, but both tests highlight the strong difference in the crystallinity degree. It is also interesting to note that after the first heating process, both the T_m and ΔH_m values of the fibers are considerably lowered. The melting temperature of the fibers in the second heating scan is 134°C, while the crystallinity degree is around 49% (i.e. 12% points higher than that detected for LLDPE). From the T_m difference in the first heating scan between LLDPE and DSK99 fibers, it is evident that there is a good temperature window (about 25°C) in which the SPCs could be produced. It is thus clear that an evaluation of the loss of performance of DSK after the thermal processing is of utmost importance. Therefore, DSK fibers were thermally treated at two different temperatures (135 and 140°C). From Table 2, it can be seen that the thermal processing of the fibers determines a slight decrease in the melting temperature (between 5 and 7°C) and of the crystallinity degree (between 5 and 10°C), and the loss of thermal properties is proportional to the temperature of the treatment. However, it can be concluded that both the T_m and ΔH_m drop induced by the temperature is not dramatic,

Table 2. Results of the DSC test on the neat PE matrix and on UHMWPE fibers as received, treated at 135°C and at 140°C.

Sample	First scan			Second scan		
	T_m (°C)	ΔH_m (J/g)	X_c (%)	T_m (°C)	ΔH_m (J/g)	X_c (%)
PE	121.2	113.0	39.0	121.0	107.2	37.0
DSK99	147.7	264.6	91.2	134.0	142.6	49.2
DSK99_135°C	142.1	249.0	85.8	122.9	134.6	46.4
DSK99_140°C	140.3	234.6	80.9	122.5	125.8	43.4

DSC: differential scanning calorimetry; PE: polyethylene; UHMWPE: ultra-high molecular weight polyethylene.

T_m : melting temperature, ΔH_m : melting enthalpy, X_c : crystallinity degree.

Table 3. Results of the tensile tests on the matrix samples (PE, OPT) and on UHMWPE fibers as received, treated at 135°C and at 140°C.

Sample	E (GPa)	σ_y (MPa)	σ_b (GPa)	ε_b (%)
PE	0.19 ± 0.04	9.8 ± 0.2	0.017 ± 0.002	1446 ± 198
OPT	0.43 ± 0.02	11.1 ± 0.1	0.010 ± 0.002	822 ± 133
DSK99	138 ± 3	–	3.7 ± 0.2	3.6 ± 0.6
DSK99_135°C	132 ± 23	–	3.2 ± 0.3	3.4 ± 0.3
DSK99_140°C	130 ± 24	–	3.2 ± 0.6	3.4 ± 0.8

OPT: PE composite with optimized composition; PE: polyethylene.

and the fibers are able to retain the greatest part of their pristine thermal properties.

It was widely demonstrated that a loss in the thermal properties of polymeric fibers upon a temperature increase is generally accompanied by a worsening of their mechanical performance. Therefore, to investigate the mechanical behaviour of the produced SPCs, it is important to determine the mechanical properties of the constituents. Table 3 reports the results of the tensile tests on the matrix samples (PE, OPT) and on UHMWPE fibers (both as received and thermally treated). As already reported in our previous paper,⁵³ the simultaneous introduction of both fumed silica and Mg(OH)₂ particles in the proper relative amount determines an important increase in the elastic modulus and of the stress at yield (σ_y), without a dramatic deterioration of the failure properties. In fact, both the σ_b and ε_b values of the OPT sample remain at an acceptable level with respect to the PE matrix. These results are in good agreement with those reported in literature for similar systems^{13,52} and can be attributed to the restriction of the motion of polymer chains due to the presence of the inorganic particles.⁵³ On the other hand, it has also to be considered that in SPCs, the tensile properties are mainly determined by the mechanical performance of the reinforcement. In this view, the observed decrease in the failure properties of the polymer matrix can be considered acceptable. It has also to be observed

that the thermal treatment of the fibers does not determine a substantial reduction of the mechanical performance of the fibers. Considering the standard deviation values, it can be concluded that both the elastic (E) and the failure properties (σ_b , ε_b) of the thermally treated fibers are not significantly different from those of the untreated DSK99 fibers. Therefore, the T_m and X_c drop experienced in DSC tests for the DSK99_135°C and DSK99_140°C samples does not determine a detectable deterioration in the reinforcing capability of the fibers.

After this characterization activity, it was decided to prepare the SPCs samples applying a hot-pressing temperature of 140°C. In fact, this temperature does not correspond exactly to a given decrease of mechanical properties but allows an improvement in the processability of the material, by lowering the viscosity of the matrix. This was also proved by the low volume fraction of pores detected in the composites (see 'Characterization of the SPCs'; Table 4).

Characterization of the SPCs

To assess the mechanical behaviour of the produced SPCs, it is important to determine the real concentration of the constituents within the composites,

Table 4. Fiber volume fraction (φ_f), theoretical density (ρ_{th}), experimental density (ρ_{exp}) and porosity of the SPC-PE and SPC-OPT composite laminates.

Sample	φ_f (vol %)	ρ_{th} (g/cm ³)	ρ_{exp} (g/cm ³)	Porosity (vol %)
SPC-PE	16.8	0.939	0.919 ± 0.021	2.1
SPC-OPT	15.4	1.049	1.035 ± 0.028	1.3

SPC-OPT: Single polymer composites-OPT; SPC-PE: Single polymer composites-polyethylene.

which was achieved through density measurements. In Table 4, the fiber volume fraction, the density (both theoretical and experimental) and porosity values of the SPC-PE and SPC-OPT laminates are compared. It is important to underline that the experimental density values of the prepared composites are very close to the theoretical ones, meaning that the pores concentration is very limited. From Table 4, it is evident that in both laminates, the porosity is very low (2.1 and 1.3% for the SPC-PE and SPC-OPT composites, respectively), meaning that the adopted hot compaction process was efficient. It is also important to notice that the prepared laminates show similar fiber concentration (16.8% and 15.4% for the SPC-PE and SPC-OPT composites, respectively). On the basis of these results, it can be concluded that the mechanical properties of the two SPCs can be directly compared.

It is now important to evaluate the thermal degradation resistance of the prepared SPCs and to compare it with that shown by the corresponding matrices. In Figure 2(a) and (b), representative TGA thermograms of the PE, OPT, SPC-PE and SPC-OPT samples are expressed in terms of residual mass and derivative of the mass loss, respectively, while Table 5 summarizes

Table 5. Results of the OOT and TGA tests on the prepared samples.

Sample	OOT (°C)	T_{onset} (°C)	T_{peak} (°C)
PE	214.5	346.2	395.3
OPT	238.2	483.3	
SPC-PE	192.7	360.6	399.2
SPC-OPT	224.7	390.8	484.6

SPC-OPT: Single polymer composites-OPT; SPC-PE: Single polymer composites-polyethylene; OOT: oxidation onset temperature; TGA: thermogravimetric analysis.

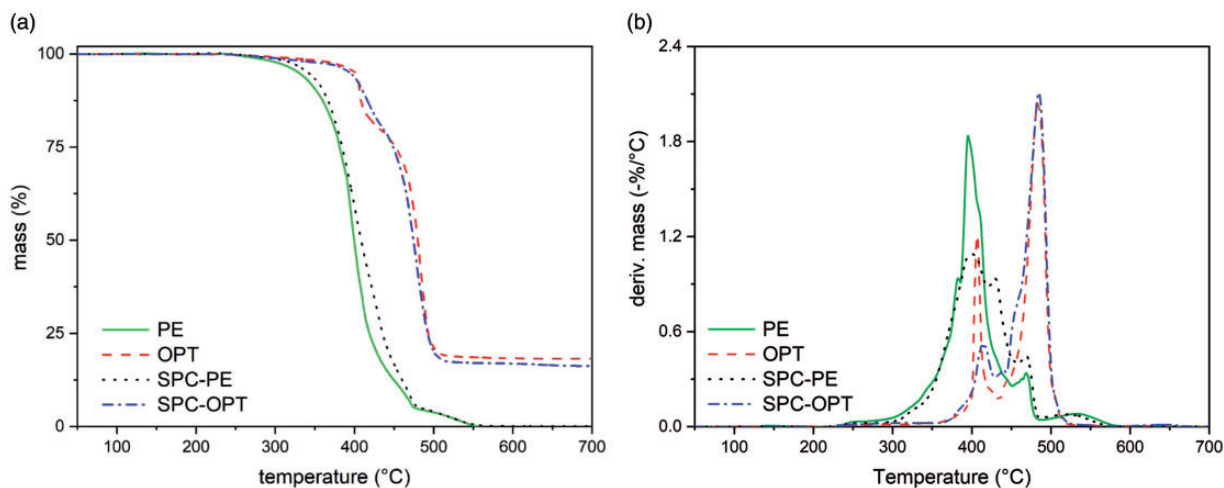


Figure 2. TGA thermograms of the PE, OPT, SPC-PE and SPC-OPT samples. (a) Residual mass and (b) derivative of the mass loss. OPT: PE composite with optimized composition; SPC-PE: single polymer composite with neat PE matrix; SPC-OPT: single polymer composite with OPT matrix.

the most important results of these tests. From the mass loss curves (Figure 2(a)), it is immediately evident that both SPCs behave like their corresponding matrices, even though from the mass loss rate plots (Figure 2(b)), it can be seen that the peak of the mass loss derivative at about 400°C is strongly reduced in SPCs samples. This behaviour can be explained considering that DSK99 fibers, due to their higher crystallinity degree, have a higher thermal degradation resistance with respect to LLDPE. This evidence is confirmed by the fact that both SPCs in mass loss rate curves show two distinct degradation steps, at about 400 and 500°C. As already observed in our previous work,³³ the introduction of both fumed silica and metal hydroxides at the optimal concentration determines a strong increase both in the onset degradation temperature (+47°C) and in the T_{peak} (+90°C). The increased thermal stability of polymer matrices due to the addition of nanofillers is generally ascribed to the fact that the nanofiller accumulates and agglomerates on the surface of the degrading polymer, creating a protective barrier that delays the volatilization of the low molecular weight degradation products.^{30,54} The beneficial effect provided by the combination of the two fillers is also transferred in SPCs. In fact, SPC-OPT sample shows a T_{onset} increase of 30°C and a T_{peak} enhancement of 85°C with respect to the SPC-PE composite.

The improvement in thermal stability provided by fumed silica and metal hydroxide particles is confirmed by OOT measurements. As reported in Table 5, OOT values measured for the two SPCs produced are lower than those obtained for the corresponding matrices. This result can be explained by considering the way in which the samples are prepared. By cutting the small portions of material to be introduced in the aluminum crucible, the SPCs were subjected to delamination under the high shear stress applied. Therefore, the surface in contact with the oxidative atmosphere increased, thereby leading to a decrease in the OOT value. However, it can be therefore noted that the SPC-OPT shows a higher OOT value than SPC-PE, with a relative increase of about 32°C. This enhancement is even higher than that shown by the comparison between OPT and PE matrices.

The introduction of fillers able to improve thermal degradation resistance and simultaneously preserve or even improve the mechanical performance of the SPCs could be very attractive from an applicative point of view. Figure 3(a) and (b) reports representative stress-strain curves obtained in the tensile tests on the SPC-PE and SPC-OPT samples in longitudinal and transversal direction, respectively, while Table 6 shows the most important tensile properties. The plots evidence the anisotropy of the prepared laminates. In

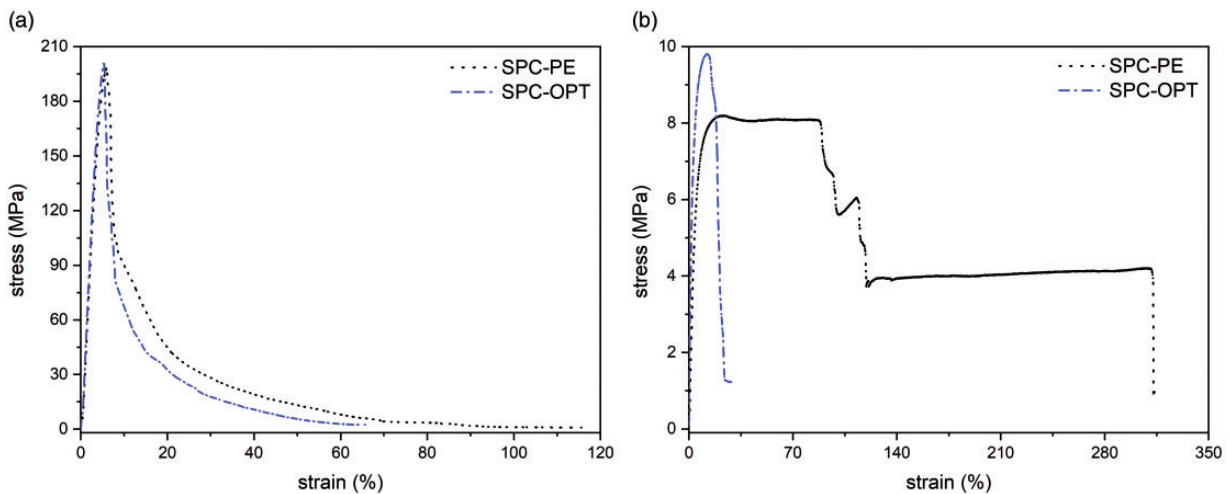


Figure 3. Representative stress-strain curves obtained in the tensile tests on the SPC-PE and SPC-OPT samples. (a) Longitudinal (fiber) direction; (b) transversal direction.

SPC-OPT: single polymer composites-OPT; SPC-PE: single polymer composites-polyethylene.

Table 6. Results of quasi-static tensile test on the prepared SPCs.

Sample	E_L (MPa)	E_T (MPa)	$\sigma_{y,L}$ (MPa)	$\sigma_{y,T}$ (MPa)	$\varepsilon_{b,L}$ (%)	$\varepsilon_{b,T}$ (%)	TEB_L (J/mm ²)	TEB_T (J/mm ²)
SPC-PE	4498 ± 62	191 ± 6	168 ± 31	8.1 ± 0.2	127 ± 18	320 ± 10	0.95 ± 0.14	0.66 ± 0.17
SPC-OPT	4844 ± 28	234 ± 29	180 ± 14	9.8 ± 0.3	86 ± 4	30 ± 5	0.87 ± 0.08	0.08 ± 0.01

SPC-OPT: Single polymer composites-OPT; SPC-PE: Single polymer composites-polyethylene.

longitudinal direction, the SPCs are stiffer and stronger, at the expenses of a reduction of the strain at break (i.e. of the ductility). It has been already observed that the additivition of both nanosilica and metal hydroxides particles on the matrices leads to an important increase in stiffness, with an acceptable reduction of the failure properties (see Table 3).³³ These effects are still present in the SPCs. It can be noticed that SPC-OPT sample shows an increase in the elastic modulus with respect to the SPC-PE laminate, both in longitudinal (+7.7%) and in transversal direction (+22.5%). Considering that the prepared composites were unidirectional, it is clear that the increase in stiffness due to the fillers addition, evaluated in transversal direction, is more intense than that measured longitudinally. Knowing the fiber volume fraction in the composites and the mechanical properties of the constituents, a theoretical value for the elastic modulus in L-direction was calculated by using the mixture rule. For both SPCs, theoretical elastic modulus would result approximately 20 GPa, considerably higher than the measured modulus. The discrepancy between this theoretical prediction and the experimental values can be partly explained by the fact that the fibers are not perfectly parallel and oriented in the loading direction: during the hot compaction of SPCs, the matrix flows towards the outside of the mold and moves the fibers from their original position.

Also, the stress at yield is positively improved upon filler additivition, with a relative increase of 7.1% in L-direction and of the 21.0% in the T-direction. Similarly to what happens in matrix samples, SPC-OPT composites show a reduction of the strain at break. Even though this reduction can be acceptable in longitudinal direction (-32.2%); in transversal direction, a harsher drop can be detected. Consequently, longitudinal ductility (i.e. TEB value) of the SPC-OPT sample is very near to that of the SPC-PE laminate, while in transversal direction, TEB values are strongly reduced. Once again, a better preservation of the fiber alignment during the hot compaction process could partially solve this problem.

It is now important to investigate the flame behaviour of the produced SPCs. Therefore, LOI tests were performed. In Table 7, the results of LOI tests are presented, together with the values of the flame propagation rate in air. It has been already reported that LOI value for the OPT sample is much higher with respect of the neat PE, being 35.2% and 18.5%, respectively.³³ It is interesting to note that SPC-PE shows a slight increase in the LOI value with respect to the corresponding matrix, because of the higher thermal stability of the DSK99 fibers, while the opposite happens for the SPC-OPT laminate. In fact, LOI registered for the SPC-OPT sample is about 10% points lower

Table 7. LOI and propagation rate in air of the prepared samples.

Sample	LOI (%)	Propagation rate in air (mm/s)
PE	18.5	0.43
OPT	35.2	n.d. ^a
SPC-PE	20.9	0.37
SPC-OPT	25.6	n.d. ^a

^aNot detectable.

SPC-OPT: Single polymer composites-OPT; SPC-PE: Single polymer composites-polyethylene; OPT: PE composite with optimized composition.

than that of the OPT matrix. This result can be explained by considering that during the cutting operations of the testing samples, the layers of the reinforcement resulted to be deprived by the protection given by the OPT matrix. This aspect influences the LOI experiment, since the propagation of the fire in the SPC-OPT specimens is quicker along the sample edges, where the fibers are exposed. Moreover, the poor interfacial cohesion between the fibres and the matrix allows the decomposition products and oxygen to diffuse along the interface during the combustion. However, what is important is that SPC-OPT shows an LOI value that is almost 5% points higher than of the SPC-PE, which indicates that, even in this testing conditions, the amount of fire retardants is sufficient for this material not to self-sustaining the flame in air. Moreover, in a possible application of these composite for engineering materials, it has to be considered that the reinforcement will be completely protected and surrounded by the matrix, which limits the problem of the lateral propagation of the flame. The beneficial effect provided by fillers addition both in the matrices and in the SPCs is confirmed by the fact that both for OPT and SPC-OPT samples, it was not possible to measure the values of the propagation rate in air, because they were too small to be detected.

One of the most important experimental techniques to evaluate the flame behaviour of polymer composites is the cone calorimetry. Figure 4(a) reports the HRR as a function of time of all the samples, while in Figure 4(b), the trends of the THR are summarized. Table 8 lists the most important results of the cone calorimeter experiments. The role played by fumed silica and metal hydroxides in decreasing the peak HRR has been already observed in our previous paper.³³ It is interesting to observe that SPC-PE has a better flame behaviour with respect to the corresponding PE sample. In fact, a strong reduction of the pHRR and of the THR can be detected. Once

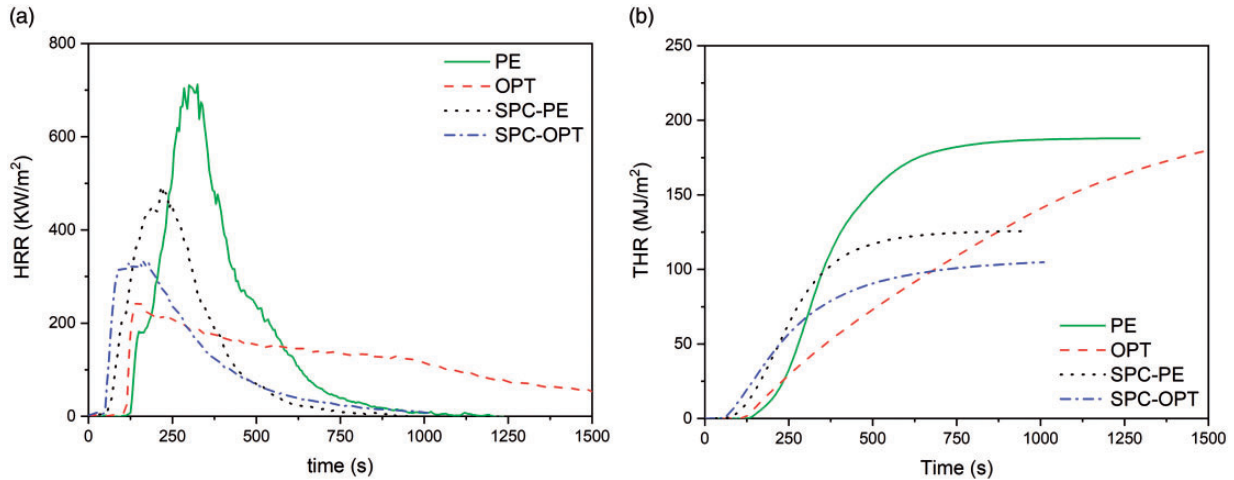


Figure 4. Cone calorimetry curves of PE, OPT, SPC-PE and SPC-OPT samples. (a) HRR as a function of time and (b) total heat released as a function of time.

HRR: heat release rate.

Table 8. Results of the cone calorimetry test on the prepared samples.

Sample	TTI (s)	pHRR (kW/m ²)	THR (MJ/m ²)	FP _i	FIGRA (kW/s m ²)	mAHRE (kW/m ²)
PE	129	712	188	0.18	2.2	311
OPT	115	246	181	0.47	1.6	147
SPC-PE	59	491	126	0.12	2.2	281
SPC-OPT	51	336	105	0.15	2.0	227

FIGRA: fire growth rate; FP_i: fire performance index (FP_i = TTI/pHRR); mAHRE: maximum of average heat release emission; pHRR: peak of heat-release rate; THR: total heat released; TTI: time-to-ignition.

again, this effect is due to the higher crystallinity degree of the DSK99 fibers. Also, the restriction of molecular mobility due to the presence of the UHMWPE could account for these results. The slight lowering of the TTI values observed in SCP-OPT with respect to the SPC-PE sample can be due to the poor quality of interface, which creates shortcuts of diffusion of volatiles and oxygen. It is important to underline that the pHRR value of the SPC-OPT laminate is higher than that of the corresponding OPT matrix, because in these laminates, the fibers represent the weak point, as already observed in the LOI tests. The SPC-OPT composite has a lower pHRR (336 kW/m²) and THR (105 MJ/m²) with respect to the SPC-PE, and thus its FP_i is higher. Moreover, the FIGRA and the mAHRE values of the SPC-OPT laminate are also lower than those detected for SPC-PE. These results confirm that the synergistic effect played by the addition of nanosilica and Mg(OH)₂ in LLDPE can also be transferred in SPCs, with important implications on the fire safety of composite structures.

Conclusions

For the first time, PE-based single polymer composites with improved flame-resistance properties were developed. The synergistic effect of fumed nanosilica and metal hydroxides was exploited to produce a LLDPE flame-resistant matrix, which was then reinforced with UHMWPE fibers. Thanks to the selection of the proper processing parameters, it was possible to prepare SPCs with a limited porosity, in which the reinforcement retained the pristine mechanical properties. SPC-OPT sample showed an increase in the elastic modulus with respect to the SPC-OPT laminate, both in longitudinal (+7.7%) and in transversal direction (+22.5%) associated to a reduction of the strain at break, especially in transversal direction. The elastic modulus in the L-direction was lower than those expected by considering the fiber volume fraction and the stiffness of the constituents, which was partly due to the fiber misalignment during the hot-pressing phase.

The beneficial effect provided by the combination of the two fillers on the thermal resistance and flame behaviour of LLDPE matrix was also transferred in SPCs, with positive outcomes on the fire safety of composite structures. In fact, from TGA tests, it was demonstrated that SPC-OPT sample showed a T_{onset} increase of 30°C and a T_{peak} enhancement of 85°C with respect to the SPC-PE composite, coupled with a higher OOT value (about 32°C). Moreover, the LOI value of SPC-OPT was almost 5% points higher than of the SPC-PE. Cone calorimetry tests highlighted that SPC-OPT composite had a lower pHRR and THR (and thus a higher FP_i) with respect to the SPC-PE laminate.

Acknowledgements

Mr Andrea De Col is gratefully acknowledged for his support to the experimental work. Dr Mauro Bortolotti and Dr Evgeny Borovin are gratefully acknowledged for their support with the XRD tests. Mr Loic Dumazert is gratefully acknowledged for cone calorimetry tests. The authors would like to acknowledge Mr Ugo Guarneri (Eurotex srl, Pietramurata, Italy) for the kind provision of DSK99 fibers.

Declaration of conflicting interests

The author(s) declared no potential conflicts of interest with respect to the research, authorship, and/or publication of this article.

Funding

The author(s) received no financial support for the research, authorship, and/or publication of this article.

ORCID iD

Giulia Fredi  <http://orcid.org/0000-0001-9987-1786>

References

- Chanda M. *Plastics technology handbook*. 5th ed. Boca Raton, FL: CRC Press – Taylor&Francis Group, 2017.
- Bar M, Alagirusamy R and Das A. Flame retardant polymer composites. *Fibers Polym* 2015; 16: 705–717.
- Dorigato A and Pegoretti A. (Re)processing effects on linear low-density polyethylene/silica nanocomposites. *J Polym Res* 2013; 20: 1773–1785.
- Malpass D. *Introduction to industrial polyethylene: properties, catalysts, and processes*. 1st ed. Salem, MA, USA: Wiley-Scrivener, 2010.
- Camino G, Costa L and Luda di Cortemiglia MP. Overview of fire retardant mechanisms. *Polym Degrad Stab* 1991; 33: 131–154.
- Laoutid F, Bonnaud L, Alexandre M, et al. New prospects in flame retardant polymer materials: from fundamentals to nanocomposites. *Mater Sci Eng R: Rep* 2009; 63: 100–125.
- Dasari A, Yu Z-Z, Cai G-P, et al. Recent developments in the fire retardancy of polymeric materials. *Prog Polym Sci* 2013; 38: 1357–1387.
- Shaw SD, Blum A, Weber R, et al. Halogenated flame retardants: do the fire safety benefits justify the risks? *Rev Environ Health* 2010; 25: 261–305.
- Aschberger K, Campia I, Pseudo LQ, et al. Chemical alternatives assessment of different flame retardants – a case study including multi-walled carbon nanotubes as synergist. *Environ Int* 2017; 101: 27–45. DOI: 10.1016/j.envint.2016.12.017.
- Waaijers SL, Kong D, Hendriks HS, et al. Persistence, bioaccumulation, and toxicity of halogen-free flame retardants. In: Whitacre DM (ed.) *Reviews of environmental contamination and toxicology*. New York, NY: Springer, 2013, pp.1–71.
- Rothon RN and Hornsby PR. Flame retardant effects of magnesium hydroxide. *Polym Degrad Stab* 1996; 54: 383–385.
- Hornsby PR. The application of hydrated mineral fillers as fire retardant and smoke suppressing additives for polymers. *Macromol Symp* 2011; 108: 203–219.
- Zaghloul MMY and Zaghloul MMY. Influence of flame retardant magnesium hydroxide on the mechanical properties of high density polyethylene composites. *J Reinf Plast Compos* 2017; 36: 1802–1816.
- Zaikov GE and Lomakin SM. Ecological issue of polymer flame retardancy. *J Appl Polym Sci* 2002; 86: 2449–2462.
- Ren F, Zhang X, Wei Z, et al. Effect of particle size and content of magnesium hydroxide on flame retardant properties of asphalt. *J Appl Polym Sci* 2013; 129: 2261–2272.
- Kim S. Flame retardancy and smoke suppression of magnesium hydroxide filled polyethylene. *J Polym Sci B Polym Phys* 2003; 41: 936–944.
- Titelman GI, Gonen Y, Keidar Y, et al. Discolouration of polypropylene-based compounds containing magnesium hydroxide. *Polym Degrad Stab* 2002; 77: 345–352.
- Hong CH, Lee YB, Bae JW, et al. Tensile properties and stress whitening of polypropylene/polyolefin elastomer/magnesium hydroxide flame retardant composites for cable insulating application. *J Appl Polym Sci* 2005; 97: 2311–2318.
- Xu Z-S, Yan L and Chen L. Synergistic flame retardant effects between aluminum hydroxide and halogen-free flame retardants in high density polyethylene composites. *Proc Eng* 2016; 135: 631–636.
- Pan Y, Han L, Guo Z, et al. Improving the flame-retardant efficiency of aluminum hydroxide with fullerene for high-density polyethylene. *J Appl Polym Sci* 2017; 134: 134–142.
- Visakh PM and Yoshihiko A (eds) *Flame retardants. Polymer blends, composites and nanocomposites*. 1st ed. Switzerland: Springer International Publishing, 2015.
- Yen Y-Y, Wang H-T and Guo W-J. Synergistic effect of aluminum hydroxide and nanoclay on flame retardancy and mechanical properties of EPDM composites. *J Appl Polym Sci* 2013; 130: 2042–2048.
- Sabet M, Hassan A and Ratnam CT. Effect of zinc borate on flammability/thermal properties of ethylene vinyl acetate filled with metal hydroxides. *J Reinf Plast Compos* 2013; 32: 1122–1128.
- Qian Y, Zhu X, Li S, et al. Flame-retardant properties of ethylene-vinyl acetate/oil sludge/fumed silica composites. *RSC Adv* 2016; 6: 63091–63098.
- Chen X, Jiang Y, Liu J, et al. Smoke suppression properties of fumed silica on flame-retardant thermoplastic polyurethane based on ammonium polyphosphate. *J Therm Anal Calorim* 2015; 120: 1493–1501.
- Courtat J, Melis F, Taulemesse J-M, et al. Effect of phosphorous-modified silica on the flame retardancy of polypropylene based nanocomposites. *Polym Degrad Stab* 2015; 119: 260–274.

27. Fu M and Qu B. Synergistic flame retardant mechanism of fumed silica in ethylene-vinyl acetate/magnesium hydroxide blends. *Polym Degrad Stab* 2004; 85: 633–639.
28. Jiao C-M and Chen X-L. Influence of fumed silica on the flame-retardant properties of ethylene vinyl acetate/aluminum hydroxide composites. *J Appl Polym Sci* 2011; 120: 1285–1289.
29. Dorigato A, Pegoretti A and Penati A. Linear low-density polyethylene/silica micro- and nanocomposites: dynamic rheological measurements and modelling. *Exp Polym Lett* 2010; 4: 115–129.
30. Dorigato A, Pegoretti A and Frache A. Thermal stability of high density polyethylene-fumed silica nanocomposites. *J Therm Anal Calorim* 2012; 109: 863–873.
31. Dorigato A and Pegoretti A. Tensile creep behaviour of polymethylpentene/silica nanocomposites. *Polym Int* 2010; 59: 719–724.
32. Dorigato A, D'Amato M and Pegoretti A. Thermo-mechanical properties of high density polyethylene - fumed silica nanocomposites: effect of filler surface area and treatment. *J Polym Res* 2012; 19: 9889–9899.
33. Fredi G, Dorigato A, Fambri L, et al. Synergistic effects of metal hydroxides and fumed nanosilica fire retardants for polyethylene. *Flame Retard Therm Stab Mater*, in press.
34. Dorigato A and Pegoretti A. Biodegradable single polymer composites from polyvinylalcohol. *Colloid Polym Sci* 2012; 290: 359–370.
35. Alcock B, Cabrera N, Barkoula N, et al. The mechanical properties of woven tape all-polypropylene composites. *Compos Part A* 2007; 38: 147–161.
36. Deng M and Shalaby SW. Properties of self-reinforced ultra-high-molecular-weight polyethylene composites. *Biomaterials* 1997; 18: 645–655.
37. Mosleh M, Suh NP and Arinez J. Manufacture and properties of a polyethylene homocomposite. *Compos Part A* 1998; 29A: 611–617.
38. Capiati NJ and Porter RS. The concept of one polymer composites modeled with high density polyethylene. *J Mater Sci* 1975; 10: 1671–1677.
39. Ogawa T, Mukai H and Osawa S. Mechanical properties of ultrahigh-molecular-weight polyethylene fiber-reinforced PE composites. *J Appl Polym Sci* 1998; 68: 1431–1439.
40. Houshyar S and Shanks RA. Mechanical and thermal properties of flexible poly(propylene) composites. *Macromol Mater Eng* 2006; 291: 59–67.
41. Barkoula NM, Peijs T, Schimanski T, et al. Processing of single polymer composites using the concept of constrained fibers. *Polym Compos* 2005; 26: 114–120.
42. Gilbert JL, Ney DS and Lautenschlager EP. Self-reinforced composite poly(methyl methacrylate): static and fatigue properties. *Biomaterials* 1995; 16: 1043–1055.
43. Hine PJ, Astruc A and Ward IM. Hot compaction of polyethylene naphthalate. *J Appl Polym Sci* 2004; 93: 796–802.
44. Pegoretti A, Zanolli A and Migliaresi C. Preparation and tensile mechanical properties of unidirectional liquid crystalline single-polymer composites. *Compos Sci Technol* 2006; 66: 1970–1979.
45. Bocz K, Bárany T, Toldy A, et al. Self-extinguishing polypropylene with a mass fraction of 9% intumescent additive – a new physical way for enhancing the fire retardant efficiency. *Polym Degrad Stab* 2013; 98: 79–86.
46. Bocz K, Toldy A, Kmetty A, et al. Development of flame retarded self-reinforced composites from automotive shredder plastic waste. *Polym Degrad Stab* 2012; 97: 221–227.
47. Seyhoglu H and Dogan M. Production and characterization of flame retardant all-polyamide composites by a film-stacking method. *Polym Polym Compos* 2015; 23: 461–466.
48. Van Krevelen DW. *Properties of polymers*. 3rd ed. Amsterdam (Netherlands): Elsevier, 1990.
49. ASTM D792 – Standard Test Methods for Density and Specific Gravity (Relative Density) of Plastics by Displacement.
50. Lutterotti L, Bortolotti M, Ischia G, et al. Rietveld texture analysis from diffraction images. *Z Kristallogr Suppl* 2007; 26: 125–130.
51. Van der Werff H and Heisserer U. High-performance ballistic fibers. *Adv Fibrous Compos Mater Ballistic Protect* 2016; 71–107.
52. Liu S-P. Flame retardant and mechanical properties of polyethylene/magnesium hydroxide/montmorillonite nanocomposites. *J Indus Eng Chem* 2014; 20: 2401–2408.
53. Dorigato A, Dzenis Y and Pegoretti A. Filler aggregation as a reinforcement mechanism in polymer nanocomposites. *Mech Mater* 2013; 61: 79–90.
54. Zhao C, Qin H, Gong F, et al. Mechanical, thermal and flammability properties of polyethylene/clay nanocomposites. *Polym Degrad Stab* 2005; 87: 183–189.